Supplementary Material for "Un-evenly distributed pixel-based camouflage metasurface hiding multi-wavelength holograms in color printing"

YAQIN ZHENG,[2] YUAN LIAO,[1] YULONG FAN,[1] LEI ZHANG,[3] ZHANG-KAI ZHOU,[2*] AND DANGYUAN LEI[1*]

[1]*Department of Materials Science and Engineering, Centre for Functional Photonics, and Hong Kong Branch of National Precious Metals Material Engineering Research Centre, City University of Hong Kong, 83 Tat Chee Avenue, Hong Kong 999077, China*

[2]*State Key Laboratory of Optoelectronic Materials and Technologies, School of Physics, Sun Yat-sen University, 510275 Guangzhou, China*

[3]*School of Electronic Science and Engineering, Xi'an Jiaotong University, Xi'an 710049, P.R. China*

*E-mail: zhouzhk@mail.sysu.edu.cn; dangylei@cityu.edu.hk

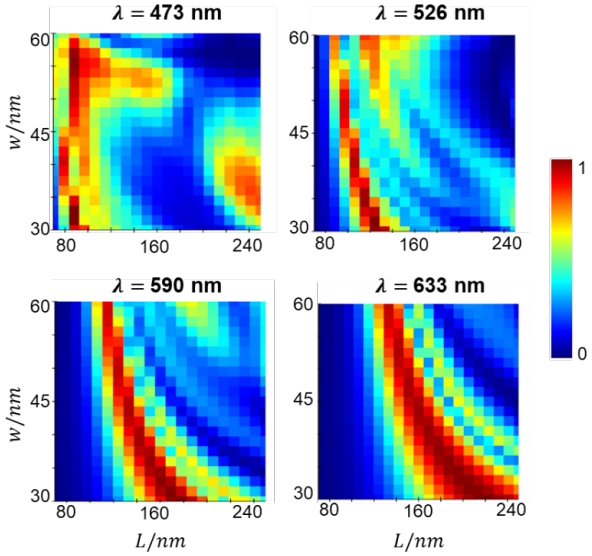

Fig. S1. Dependence of cross-polarized transmission on the parameters of width and length for four target wavelengths. Incident light is circularly polarized.

Note: We consider crosstalk to be negligible when the target signal intensity is three times that of the non-target signal intensity. Therefore, the spectral bandwidth of the nanopillars corresponding to the 633, 532, and 473 nm wavelengths should not be too broad. From Fig. S1, we can conclude that the selection of the nanopillars is appropriate, ensuring that the efficiency at non-target wavelengths satisfies the aforementioned conditions. Since the nanopillars corresponding to the 594 nm are spatially separated, we do not need to consider their bandwidth.

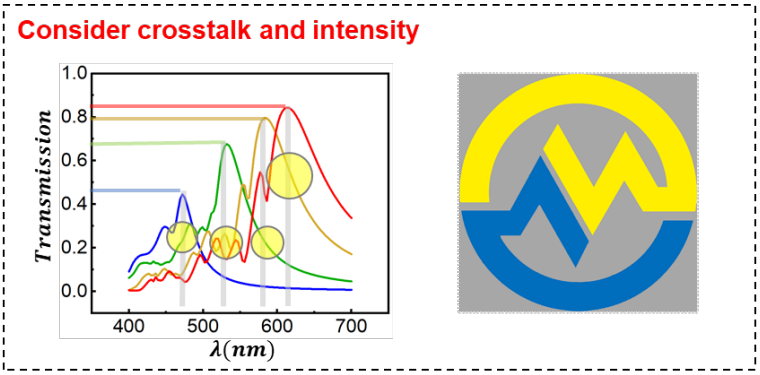

Channel (nm)	T	S	Crosstalk affect	D	Distribution
473	L	H	Green	H	Simplex + Complex
532	M	M	Yellow and blue	L	Complex
594	M	L	Green and red	M	Simplex
633	H	M	Yellow	L	Complex

Note: $I_c = T \cdot D \cdot S$, L-Low, H-High, M-mid

Table S1. A combination of crosstalk and channel strength is used to determine the density of the meta-atoms and how the pixels are combined. T is the transmittance of one meta-atom, D is the density and S is the area of a meta-atom of the same size. I_c is the total transmission intensity of each UEDP. Simplex indicates UEDPs supporting only one color, while complex indicates UEDPs supporting a mixed color, i.e., gray color.

Note: In the upper-left inset, four spectral lines resonant at four wavelengths (473, 532, 594, and 633 nm) with varying bandwidth. They overlap with adjacent resonant spectra, which result in the crosstalk. Since crosstalk of yellow signal in spectrum is inevitable, we must spatially separate the yellow signal from the green and red channels to avoid distortion of the printed image.

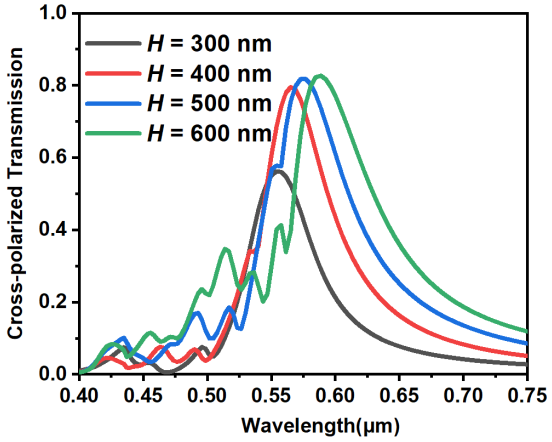

Fig. S2 Simulated transmission spectra of c-silicon nanopillars with different height H. The length, width and period are fixed (L = 140 nm, W = 40 nm, P = 300 nm).

Note: As shown in Fig. S2, a greater height of the nanopillars corresponds to a higher the intensity of the transmission peak for the respective wavelength. However, as the height increases, the enhancement of transmission efficiency becomes smaller, and the complexity of fabrication also escalates. By balancing the trade-off between fabrication difficulty and transmission efficiency, we ultimately chose 600 nm as the height of the nanopillars.

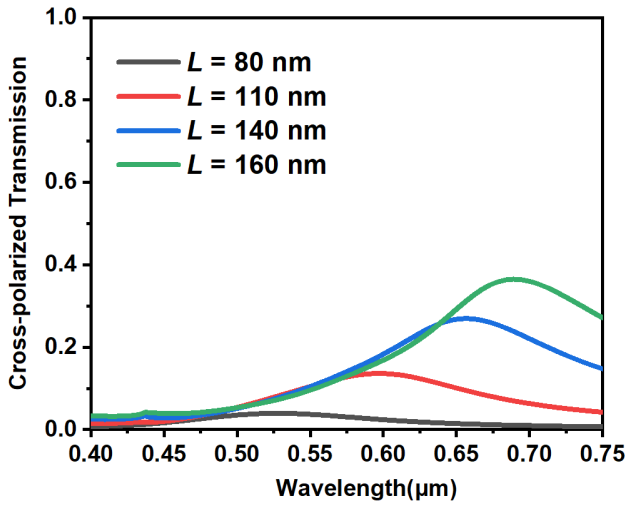

Fig. S3. Simulated transmission spectra of amorphous silicon nanopillars with different length L. The height, width and period are fixed (H = 600 nm, W = 40 nm, P = 300 nm).

Note: If we choose amorphous silicon as the material of the metasurfaces, the initial preparation could be easily accomplished by depositing an amorphous silicon film onto a glass substrate through chemical vapor deposition. However, amorphous silicon has high losses in the visible spectrum, which prevents it from achieving simultaneous manipulation across four wavelengths. As shown in Fig. S3, the blue signal would be exceedingly weak, and the bandwidth would expand, resulting in crosstalk. Consequently, we must transfer the purchased crystalline silicon (SOI wafer), despite the fact that this process is relatively complex.

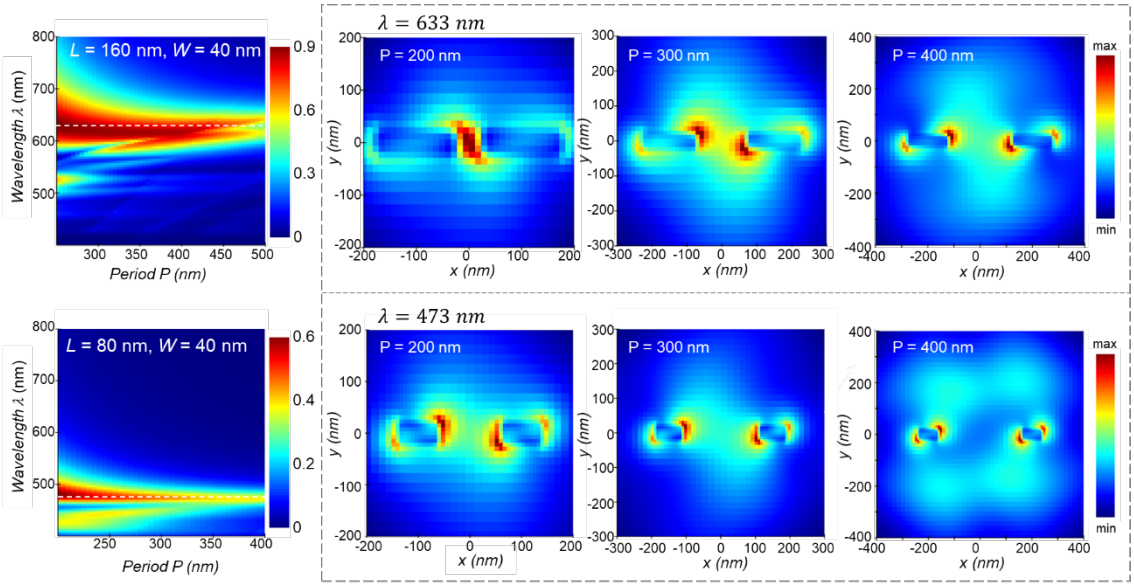

Fig. S4. Influence of period to spectral response and near-field crosstalk for 633 nm and 473 nm.

Note: The period of the meta-atoms is chosen based on these simulation results. As shown in Fig S4, using a larger period in the simulation results in a decrease in the conversion efficiency of the meta-atoms. In other words, the performance of the metasurfaces declines, which is something we aim to avoid. Conversely, if the period is too small, the interactions between adjacent nanopillars are intensified, leading to deviations from the simulation results presented in the manuscript (Fig. 2D). In this figure, we can observe that as the period decreases to 250 nm, a second transmission peak emerges. Therefore, we selected an optimal period that balances these factors. In fact, our unevenly distributed pixel not only ensure a uniform intensity distribution of colors in the printed image but also maintain the resolvability of these holograms. Thus, we can adjust the densities of the four types of nanopillars corresponding to different colors, enabling the intensities of different colors to be approximately balanced, resulting in a high-fidelity chromatic image.

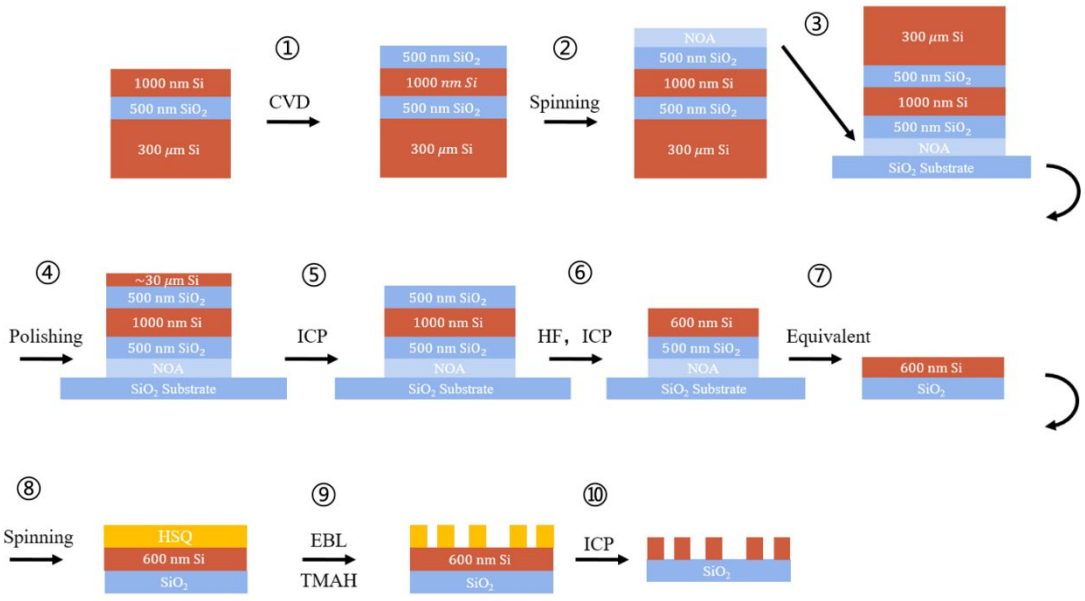

Fig. S5. The fabrication process of the camouflage metasurface. CVD, chemical vapor deposition; ICP, inductively coupled plasma; NOA, Norland Optical Adhesive 61; HF, 10% Hydrofluoric acid solution; EBL, electron beam lithography; TMAH, tetramethylammonium hydroxide.

Note: We use fused silica quartz (2 cm × 2 cm × 1 mm in length, width, and thickness, respectively) as the substrate and chose crystalline silicon as the nanostructure material due to its high refractive index and low loss. Silicon-based metasurfaces have a wide range of applications and are suitable for optoelectronic integration devices. In addition, compared to amorphous silicon, crystalline silicon has less optical loss in the blue light band, which is crucial for enhancing imaging quality.

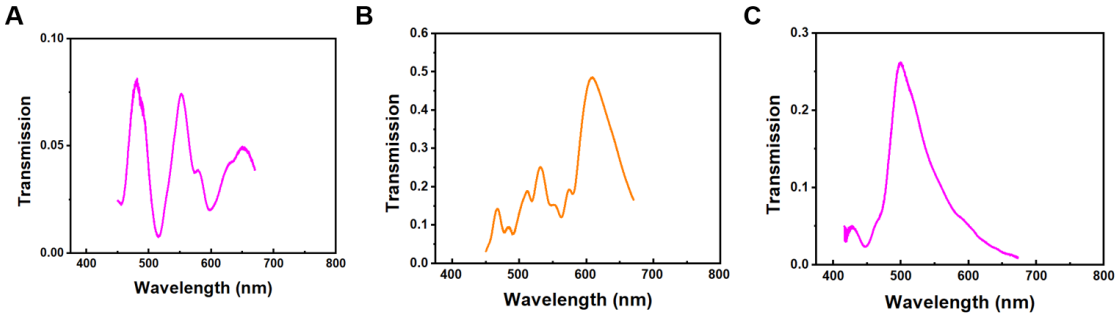

Fig. S6. Measured transmission results of three fundamental types of UEDPs with size of 1.2 μm × 1.2 μm. The period is 300 nm for the UEDPs supporting mixed color and yellow color (A and B), while 200 nm for the UEDP supporting blue color (C).

Note: The main reason for the decrease of efficiency is the experimental influence, which includes the intrinsic absorption of material, the fabrication error, the reflection of optical setup and more. For example, a typical fabrication error of 10-20 nm in size is unavoidable in the electrical beam lithography technique, potentially leading to an efficiency loss of 10-50% [Light Sci. Appl. 2019, 8, 95]. Furthermore, in our UEDP design, the metasurfaces are constructed using the pixels for four colors. Consequently, the nanopillars corresponding to a specific color cannot cover the entire metasurfaces, resulting in an additional reductio in the hologram efficiency. In the future, we can expect higher efficiency by optimizing theoretical design, selecting materials with lower losses, and enhancing the fabrication technologies.

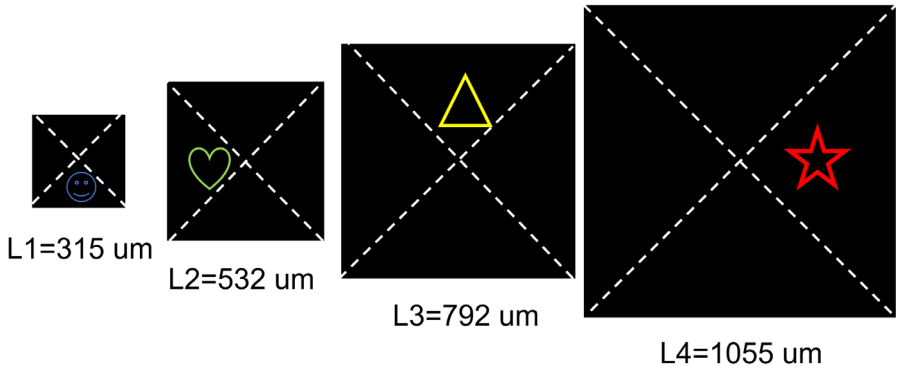

Fig. S7 The simulation results of holographic images at different diffraction angles: (-90°, 70°), (0°, 70°), (90°, 70°) and (180°, 70°). The blue, green, yellow, and red correspond to wavelengths of 473, 532, 594, and 633 nm, respectively.

Note: Theoretically, holographic images can be designed at arbitrary positions and angles using the Fresnel diffraction formula. However, considering the imaging space, non-overlapping of images, and design convenience, we have chosen imaging distances (focal length) of 800, 1200, 1600, and 2000 μm for the wavelengths 473, 532, 594, and 633 nm, respectively.

Once the focal length is determined, the size of the holographic image can be calculated using the following formula:

$$L_{holo} = z \cdot \frac{\lambda}{d}.$$

Here, L, z, λ, and d represent the size of the holographic image, the focal length, the wavelength, and the pixel period within the metasurfaces, respectively. Therefore, our design principle is to completely separate the paths and final imaging positions of the four holographic images in space. As long as this condition is met, there is considerable flexibility in choosing the image size, focal length, and spatial angles. For example, the four spatial angles, (-90°, 70°), (0°, 70°), (90°, 70°) and (180°, 70°), were defined to satisfy the aforementioned requirements. As shown in Fig. S7, simulation results demonstrate that our four holographic images do not overlap, thus satisfying the condition we discussed above.